J. Meas. Sci. Instrum., 2026, 17(2): 267-277. http://jmsi.publish.founderss.cn/
DOI: 10.62756/jmsi.1674-8042.2026023 jmsi@nuc.edu.cn

Image defogging algorithm combining SLIC super-pixel segmentation and transmission optimization

LI Jiying*, LIU Yu, LIU Jie

School of Electronic and Information Engineering, Lanzhou Jiaotong University, Lanzhou 730070, China

***Corresponding author:** LI Jiying (ljy7609@126.com)

Received: September 6, 2025 **Revised:** September 29, 2025 **Accepted:** October 2, 2025

Abstract: When images are captured under hazy conditions, light is attenuated and deflected by particle scattering, resulting in reduced brightness and color distortion, which affects the imaging quality of the visual system. This paper proposes a defogging method that combines super-pixel segmentation and transmission optimization. First, the complexity of the haze image was calculated using color entropy to adaptively determine the number of super-pixel blocks. The simple linear iterative clustering (SLIC) super-pixel segmentation method was used to obtain super-pixel blocks with the same features. And the super-pixel block with the highest score was selected as a candidate block to accurately estimate the atmospheric light value. Then, the transmission was estimated using the multiscale dark channel prior and the non-local haze-lines prior, and then the initial transmission after fusion was obtained by wavelet transform. In addition, a guided filter based on unsharp masking was introduced to further improve the transmission estimation accuracy. Finally, an atmospheric scattering model was used to invert the haze-free image. We have conducted a large number of quantitative and qualitative experiments on three datasets, and the results show that the proposed algorithm can achieve a better de-fogging effect, especially in the sky region, where the image restoration effect is more prominent.

Key words: super-pixel blocks; atmospheric light value; multiscale dark channel prior; non-local haze-lines prior; transmission fusion; unsharpened masking

0 Introduction

In harsh climatic conditions such as fog, smoke, mist, or dust, atmospheric particles can seriously affect image quality, resulting in reduced image clarity, faded colors, decreased contrast, and uneven brightness. These problems not only affect visual perception but also make it difficult for certain outdoor computer vision systems to recognize object features[1]. Therefore, the study of image defogging algorithms is of great scientific research value and practical significance in the fields of computer vision, security monitoring, automatic driving, etc[2-5].

Many image defogging techniques have been developed. Image enhancement-based defogging algorithms (i.e., histogram equalization[6], the Retinex algorithm[7], and homomorphic filtering[8]) improve the visual quality of blurred images by adjusting attributes such as contrast, brightness, and color. However, such methods fail to consider the real causes of image degradation, which may lead to color distortion and over-enhancement, and are unable to handle complex scenes. Deep learning-based defogging methods are capable of automatically learning complex feature representations with strong adaptive capabilities[9-12]. However, such methods require large amounts of labeled data and computational resources for training, resulting in high model complexity. Physical model-based approaches can be traced back to the atmospheric scattering model[13], which was further described and derived[14] and widely applied to the field of image defogging. Since then, defogging algorithms based on various prior knowledge have been proposed[15]. He et al.[16] proposed a defogging technique based on the dark channel prior, which provided a rough estimation of the transmission map and atmospheric light values. It utilizes an atmospheric scattering model to reconstruct clear images. However, in regions similar to the atmospheric light values, the transmission estimates tend to be low, resulting in oversaturated images or darkened colors. Ehsan et al.[17] combined dark-channel and atmospheric light to compute a dual transmission map, introduced a gradient-domain guiding filter to refine the transmission

© The Author(s) 2026. Published by Publishing Center of North University of China. The articles published in this open access journal are distributed under the terms of the Creative Commons Attribution 4.0 International License (http://creativecommons.org/licenses/by/4.0/), which permits use, distribution and reproduction in any medium, provided the original work is properly cited.

map, and better preserved the details and textures of the image. Hua et al.[18] utilized near-infrared (NIR) information to differentiate between sky and non-sky regions, and improved the dark-channel prior algorithm to enhance the visibility of the image. Zhong et al.[19] combined the guided filtering and adaptive tolerance mechanisms to further refine the estimation of transmission and effectively reduce the distortion of the sky region. Dwivedi et al.[20], on the other hand, took into account the effect of different color channels on the transmission by calculating the transmission of the three color channels separately and taking the average of the three color channels as the final transmission. To further improve the defogging effect, Berman et al.[21] proposed a defogging method based on non-local haze-lines prior. This method accurately estimates the transmission of each pixel by analyzing the global characteristics of the image, and performs particularly well in sky region image restoration. However, it is less effective in dense foggy regions. Nie et al.[22] combined the haze-lines prior and the dark channel prior to determine the true location of the maximally clustered haze-lines, which improves the accuracy of the end-point pixel locations and thus enhances the de-fogging effect. Jin et al.[23] enhanced the transmission estimation by fusing multi-exposure images to obtain better generalized haze-lines and introduced a weighted least-squares filter to further improve the accuracy of the transmission estimation. Due to the limitations of the prior theories, the defogged images tend to be dark overall with serious loss of details and artifacts. This paper proposes an image defogging method that combines super-pixel segmentation with transmission optimization.

A simple linear iterative clustering (SLIC) super-pixel segmentation algorithm is introduced to accurately estimate the atmospheric light value by calculating the super-pixel block score. To overcome the limitation of a fixed number of super-pixel blocks, this paper uses color entropy to calculate the image complexity, adaptively determines the number of super-pixel blocks, and selects the block with the highest score to estimate the atmospheric light value. We improve the traditional dark channel prior and non-local haze-lines prior and fuse the two by wavelet transform to obtain the coarse transmission map. Then, the coarse transmission map is subjected to unsharpened masking processing to obtain a sharpened image, which is used as the guided map for the guided filtering to improve the accuracy of the transmission estimation. And the haze-free image is restored based on the atmospheric scattering model.

1 Atmospheric scattering model

The fog generated during the imaging process will obstruct the propagation of light. Due to the same degree of scattering, light of different wavelengths will become mixed, resulting in reduced image contrast, decreased color saturation, and weakened visibility. The impact of atmospheric scattering on image degradation is analyzed and an atmospheric scattering model is proposed[13], shown as Eq. (1). From the perspective of imaging, the light that enters the acquisition device and participates in the imaging process is an important basis for understanding the degradation phenomenon of haze images. It is an important basis for understanding the degradation process of the haze image and recovering the fog-free image.

$$\boldsymbol{I}(x)=\boldsymbol{J}(x)\boldsymbol{t}(x)+\boldsymbol{A}(1-\boldsymbol{t}(x)), \tag{1}$$

where $\boldsymbol{I}(x)$ denotes the haze image; $\boldsymbol{J}(x)$ denotes the haze-free image; $\boldsymbol{A}$ denotes the global atmospheric light value, and $\boldsymbol{t}(x)$ denotes a transmission map, which represents the component of the light that is not scattered during its transmission from the object to the observer. $\boldsymbol{J}(x)\boldsymbol{t}(x)$ is the direct attenuation term, which indicates the radiated or attenuated component of the light during transmission, and $\boldsymbol{A}(1-\boldsymbol{t}(x))$ is called atmospheric light imaging, which is caused by the phenomenon of atmospheric scattering, and is susceptible to image color deviation. In a homogeneous medium, $\boldsymbol{t}(x)$ can be expressed as

$$\boldsymbol{t}(x)=\mathrm{e}^{-\beta d(x)}, \tag{2}$$

where β is the atmospheric scattering coefficient and $d(x)$ is the depth of field corresponding to the coordinates of the imaged pixel. Assuming that β remains constant at each wavelength of light, $\boldsymbol{t}(x)$ is regarded by x as the relative depth of the scene, with a value between 0 and 1. From Eq. (2), it can be seen that increasing the distance between the camera and the object leads to a decrease in $\boldsymbol{t}(x)$, which means that the effect of atmospheric light on the image increases. The goal of dehazing is to restore $\boldsymbol{J}(x)$ from the hazy image. According to Eq. (1), $\boldsymbol{J}(x)$ is restored by

$$\boldsymbol{J}(\mathrm{x})=\frac{\boldsymbol{I}(x)-\boldsymbol{A}}{\boldsymbol{t}(x)}+\boldsymbol{A}. \tag{3}$$

However, Eq. (3) is an ill-posed problem because $\boldsymbol{t}(x)$ and $\boldsymbol{A}$ are unknown variables without additional information. Therefore, the performance of the algorithms based on the atmospheric scattering model depends on the accurate estimations of $\boldsymbol{t}(x)$ and $\boldsymbol{A}$.

2 Proposed method

Although the dark channel prior algorithm performs well in defogging, the use of a rectangular filter as a defogging window leads to significant white edges in the recovered image. The non-local haze-lines prior algorithm uses the pixel values of the entire image to estimate the initial transmission, which avoids the white edge problem and is especially effective in recovering the sky region but has limited effect when dealing with dense fog regions. In order to solve the problems of white edges and color distortion in images, this paper proposes a defogging method that combines SLIC super-pixel segmentation with transmission optimization. The overall block diagram of the proposed algorithm is shown in Fig.1, which contains three main modules: atmospheric light value optimization, transmission fusion, and unsharpened masking-guided filtering. The first module introduces color entropy to calculate the complexity of the haze image and uses SLIC super-pixel segmentation to segment the haze image into multiple super-pixel blocks. Then, the mean of the pixel values within the block minus the standard deviation of the pixel values is computed to obtain the super-pixel block score, and the candidate block with the highest score is selected to accurately estimate the atmospheric light value, which enhances the dehaze effect and makes the image clearer. The second module synthesizes the advantages of the multiscale dark channel prior and the non-local haze line prior, and extracts features for multiscale analysis using wavelet transform to obtain the initial transmission. The third module performs unsharpened masking bootstrap filtering on the initial transmission to obtain the fine transmission, which enhances the electronic estimation of the transmission and effectively solves the problem of loss of details at the edges of the image. Finally, the obtained parameters are integrated into the atmospheric scattering model for defogging to generate clear, haze-free images.

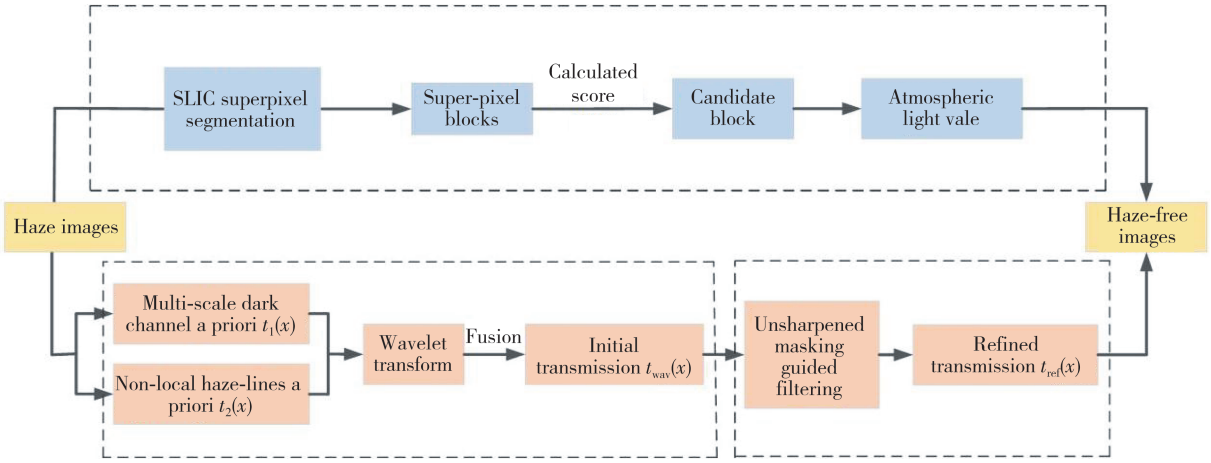


Fig. 1 Overall block diagram of proposed algorithm

2.1 Optimization of atmospheric light values

According to the atmospheric scattering model, atmospheric light reflects radiation at an infinite depth of field distance, and thus the estimated point is supposed to have a high brightness and be situated in the background region of the image[24]. However, the traditional dark channel prior algorithms adopt a global approach to estimate the atmospheric light value by selecting 0.1% of the pixels with the highest brightness from the dark channel map, subsequently mapping these selected values to the haze image, and choosing the pixel with the highest intensity as the atmospheric light for calculation[25]. To enhance the accuracy of the estimation of the atmospheric light value, the proposed method was used to estimate the atmospheric light from a local area. The specific steps are as follows.

1) SLIC super-pixel segmentation[26] is first performed on foggy images to obtain k super-pixel blocks. Through super-pixel clustering, the depth of field within the same super-pixel block is ensured to be consistent, which is in line with the dark channel prior theory. However, the existing SLIC super-pixel segmentation algorithm has a drawback, i.e., the fixed number of super-pixel blocks, k, is improperly set to affect the performance of the algorithm[27]. Too many super-pixel blocks will increase the complexity and defogging time of the algorithm, while too few will lead to poor segmentation clustering. To optimize this problem, this paper introduces a color entropy-based image complexity assessment method to adaptively determine the number of super-pixel blocks required for image segmentation. The expression of color entropy is

$$H = -\sum_{i=1}^{N} p_i \log p_i, \tag{4}$$

where H denotes the color entropy; N denotes the

number of gray levels; and p_i denotes the probability histogram of the i gray level. Since the number of super-pixels is usually related to the image size, the expression for the number of adaptive super-pixels is obtained by combining the image size and color entropy as

$$K=\left[\frac{H(r+c)}{m}\right], \tag{5}$$

where r denotes the width of the image; c denotes the length of the image; m is a constant used to adjust the number of super-pixel blocks, and the value of m is 5 in this paper.

2) Calculate the score $s(i)$ for each super-pixel block, i.e., the average pixel value within the block minus the standard deviation of the pixel values within the block. The candidate block with the highest score is selected, as marked in red in Fig.2(d).

$$s(i)=\mu(B_i)-\sigma(B_i), \tag{6}$$

where μ is the mean value and σ is the standard deviation.

3) To avoid the effect of suspended particles, the top 1% of the brightest pixels in the dark channel of the candidate block are selected instead of 0.1%, because the individual pixels corresponding to 0.1% may be noisy, leading to atmospheric light misestimation.

4) The selected pixels are mapped to the original haze image. The median value of these pixels is then calculated. The median value is chosen because it is less affected by noise or outliers. Finally, the estimated median value is used as the atmospheric light estimate.

Fig.2 shows the atmospheric light locations (marked in red) determined by the dark channel prior algorithm and the algorithm in this paper. As can be seen in Fig.2(c), the atmospheric light determined by the dark channel prior algorithm is located in the foreground region of the white building and image. However, as shown in Fig.2(d), the candidate blocks for estimating the atmospheric light are selected from the sky region and are brighter, indicating that the algorithm in this paper is able to estimate the atmospheric light values more accurately.



(a) Haze image (b) SLIC segmentation (c) DCP[16] (d) Ours

Fig. 2 Position of atmospheric light determined by different algorithms

2.2 Transmission fusion

2.2.1 Multiscale dark channel prior

Most RGB images have very low-intensity pixels in at least one color channel of the non-sky patches. When the intensity tends to zero, the color is biased toward dark or black. This phenomenon is called the dark channel. Based on this, the dark channel $\boldsymbol{J}^{\text{drak}}(x)$ of the haze-free image $\boldsymbol{J}(x)$ can be expressed as

$$\boldsymbol{J}^{\text{dark}}(x)=\min_{y\in\boldsymbol{\Omega}(x)}\left\{\min_{c\in\{r,g,b\}}(\boldsymbol{J}^c(y))\right\}\to 0, \tag{7}$$

where $\boldsymbol{J}^{\text{drak}}(x)$ is the dark primary color channel; $\Omega(x)$ is the local image block centered on pixel x; $\boldsymbol{J}^c(y)$ is a certain channel value in the RGB three channels. Assuming that the transmission is constant, written as $\tilde{\boldsymbol{t}}(x)$, combined with Eqs.(1) and (7), the transmission can be calculated by

$$\tilde{\boldsymbol{t}}(x)=1-\min_{y\in\boldsymbol{\Omega}(x)}\omega\left\{\min_{c}\left(\frac{\boldsymbol{I}^c(y)}{\boldsymbol{A}^c}\right)\right\}, \tag{8}$$

where $\boldsymbol{I}^c(y)$ represents RGB three-channel value of a channel in the fog image; $\boldsymbol{A}^c$ represents the atmospheric light value. In order to keep the image somewhat foggy, the constraint parameter ω is added to Eq.(3), which is usually taken as 0.95.

The transmission estimated using Eq.(8) has the problems of a single filter window size and an uneven selection of dark channels. Therefore, two different filter window sizes are selected according to the image size as

$$\begin{cases}\boldsymbol{\Omega}_1=\max(3,0.01r,0.01c),\\ \boldsymbol{\Omega}_2=\max(3,0.03r,0.03c),\end{cases} \tag{9}$$

where r and c are the width and height of the image, respectively.

According to Eq.(7), the dark channel corresponding to each color channel under the Ω_1 filter window is calculated separately by

$$\begin{cases}\boldsymbol{J}_{r_1}^{\text{dark}}(x)=\min\limits_{y\in\boldsymbol{\Omega}_1(x)}\left(\min\limits_{r_1}(\boldsymbol{J}^{r_1}(y))\right),\\ \boldsymbol{J}_{g_1}^{\text{dark}}(x)=\min\limits_{y\in\boldsymbol{\Omega}_1(x)}\left(\min\limits_{g_1}(\boldsymbol{J}^{g_1}(y))\right),\\ \boldsymbol{J}_{b_1}^{\text{dark}}(x)=\min\limits_{y\in\boldsymbol{\Omega}_1(x)}\left(\min\limits_{b_1}(\boldsymbol{J}^{b_1}(y))\right),\end{cases} \tag{10}$$

where J_{r_1} is the red channel of J under the Ω_1 filtered window; J_{g_1} is the green channel of J under the Ω_1 filtered window; J_{b_1} is the blue channel of J under the Ω_1 filtered window.

By combining Eqs. (8) and (10), the transmission of each color channel under the Ω_1 filter window is obtained by

$$\begin{cases} \tilde{t}_{r_1}(x)=1-\omega \min\limits_{y\in\Omega_1(x)}\left(\min\limits_{r_1}\left(\dfrac{I^{r_1}(y)}{A^c}\right)\right), \\ \tilde{t}_{g_1}(x)=1-\omega \min\limits_{y\in\Omega_1(x)}\left(\min\limits_{g_1}\left(\dfrac{I^{g_1}(y)}{A^c}\right)\right), \\ \tilde{t}_{b_1}(x)=1-\omega \min\limits_{y\in\Omega_1(x)}\left(\min\limits_{b_1}\left(\dfrac{I^{b_1}(y)}{A^c}\right)\right). \end{cases} \tag{11}$$

Similarly, according to Eqs. (10) and (11), the dark channels under the Ω_2 filter windows are $J_{r_2}^{\text{dark}}(x)$, $J_{g_2}^{\text{dark}}(x)$, $J_{b_2}^{\text{dark}}(x)$, and the corresponding transmission are $\tilde{t}_{r_2}(x)$, $\tilde{t}_{g_2}(x)$, $\tilde{t}_{b_2}(x)$, respectively. The final multiscale transmission is the average transmission of the three color channels under the two filter windows, and the expression is

$$t_1(x)=\frac{\left[\tilde{t}_{r_1}(x)+\tilde{t}_{r_2}(x)+\tilde{t}_{g_1}(x)+\tilde{t}_{g_2}(x)+\tilde{t}_{b_1}(x)+\tilde{t}_{b_2}(x)\right]}{6}. \tag{12}$$

The individual transmission of each color channel under different filter windows is calculated, taking into account the effect of the transmission of foggy images between different dark channels.

2.2.2 Non-local haze-lines prior

The non-local blurry boundaries follow this rule: in an image without fog, the color can be approximately represented by a small number of closely distributed color clusters in the RGB space. It is found that the pixels of these color clusters are usually distributed throughout the entire image plane, and their distances from the camera vary. And these different distances result in different transmission effects. With the addition of artificial fog, the previously formed clusters are no longer clustered but are drawn into a straight line. These lines are called haze-lines. The distance between each pixel point on the haze-lines and atmospheric light is defined as

$$r=\| I-A \|. \tag{13}$$

According to the non-local prior principle, the larger the radius r is, the less fog there is at the corresponding location. If there are haze-free pixels on the haze-lines, the point with the maximum haze-free distance is considered to be the largest point on the haze-lines, and its radius is written as

$$r_{\max}(x)=\max_{x\in H}\{r(x)\}. \tag{14}$$

The initial estimated transmission of the image can be expressed as

$$t(x)=\frac{r(x)}{r_{\max}(x)}. \tag{15}$$

The haze-free image can be obtained by the atmospheric scattering model. However, considering that there is a certain distance between the camera and each point in the image, these points will be affected by the fog, so $r_{\max}(x)$ should be smaller than the radius of the pixel point that is completely haze-free. In order to reflect this reality more accurately, we adjust Eq. (15) as

$$\tilde{t}(x)=\frac{r(x)}{\tilde{r}_{\max}(x)+\gamma}, \tag{16}$$

where γ is the complementary constant for sharpness adjustment.

Since $J(x)$ is positive, according to the principle of the defogging model, the minimum boundary value t_{XJ} of the initial transmission can be obtained by

$$t_{\text{XJ}}=1-\min_{c\in\{r,g,b\}}\{I_c(x)/A^c\}. \tag{17}$$

In order to avoid undesirable de-fogging effects due to too small transmission, a larger value is chosen between the estimated initial transmission and the minimum boundary value. The specific calculation procedure is

$$\tilde{t}_{\text{XJ}}(x)=\max\{\tilde{t}(x),t_{\text{XJ}}(x)\}. \tag{18}$$

The regularization model of Berman[21] is used to optimize the transmission to obtain the final transmission estimate.

$$t_2(x)=\sum_x\frac{\left[\tilde{t}(x)-\tilde{t}_{\text{XJ}}(x)\right]^2}{\delta^2(x)}+\lambda\sum_x\sum_{y\in N_x}\frac{\left[\tilde{t}(x)-\tilde{t}(y)\right]^2}{\left\| I(x)-I(y)\right\|^2}, \tag{19}$$

where $\delta(x)$ denotes the standard deviation of the predicted transmission for each haze-line, and its value increases as the number of pixels on each haze-line decreases. λ is the weighting factor, which takes the value of 0.1, and N_x represents the four-neighborhood of x.

2.2.3 Transmission fusion

In this paper, wavelet decomposition[28] is performed on two transmission maps $t_1(x)$ and $t_2(x)$ to obtain the low-frequency coefficients and high-frequency coefficients of the same scale. Then the low-frequency part is fused by weighted average to retain the average characteristics of the image and reduce the noise, and the

high-frequency part is fused by the method of larger absolute values of the coefficients to retain the details and contrast information of the image. The fused low-frequency coefficients L_f and high-frequency coefficients H_f are inverted by wavelet inversion, and the initial transmission $\boldsymbol{t}_{wav}(x)$ after fusion is obtained by

$$\boldsymbol{t}_{wav}(x)=\text{wavelet}(\boldsymbol{t}_1(x),\boldsymbol{t}_2(x)). \tag{20}$$

2.3 Unsharpened masking guided filtering

The optimization formula of the guided filtering algorithm is shown as

$$\boldsymbol{G}_t=\text{GF}(p,i,r,\varepsilon), \tag{21}$$

where $\boldsymbol{G}_t$ denotes the fine transmission; GF denotes the guided filter function; p represents a rough transmission grayscale image; i denotes the foggy image; r denotes the size of the filter kernel; ε denotes the regularization parameter.

In order to further improve the clarity and detail of the image, the guided filtering method combined with unsharp masking technique is used in this paper. The process of unsharpened masking can be expressed by

$$g(x,y)=f(x,y)+\beta\left\{f(x,y)-\text{LP}\left[f(x,y)\right]\right\}, \tag{22}$$

where $f(x,y)$ represents the original input image, which is the coarse transmission map in this paper; LP stands for lowpass filter, while in this paper, a mean filter is adopted; β is the gain coefficient of the high-frequency details; $g(x,y)$ is the output image after enhancement.

In this paper, the coarse transmission map obtained by wavelet transform fusion is firstly processed by unsharpened masking based on mean filter to obtain the sharpened image $g(x,y)$. Then, the sharpened image $g(x,y)$ is used as the guiding map of the guiding filter Eq. (21), and the guiding filter is used to process the input image, and the refined transmission map $\boldsymbol{t}_{ref}(x)$ is obtained in the end.

2.4 Haze-free image restoration

Integration of the obtained atmospheric light value $\boldsymbol{A}$ and fine transmission $\boldsymbol{t}_{ref}(x)$ into Eq. (3) yields a haze-free image, that is

$$\boldsymbol{J}(x)=\frac{\boldsymbol{I}(x)-\boldsymbol{A}}{\max(\boldsymbol{t}_{ref},t_0)}+\boldsymbol{A}, \tag{23}$$

where t_0 is the minimum value of transmission, usually taken as 0.1.

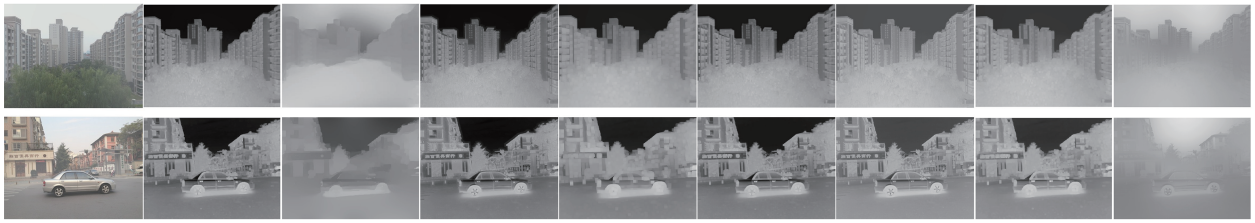
3 Results and discussion

In order to evaluate the performance of the proposed method, this paper demonstrates the defogging results on 3 sets of haze images, providing qualitative and quantitative evaluation results. The synthesis object testing set (SOTS), indoor training set (ITS), and hybrid subjective test set (HSTS) from the publicly available dataset RESIDE[29] were selected, from which images were chosen as experimental data. The experimental platform was a computer with a 64-bit Windows 11 operating system, an AMD Ryzen 5 5500U processor with Radeon Graphics, a CPU with a main frequency of 2.10 GHz, and 16 GB of RAM. The parameters of the algorithm in this paper refer to those in Refs. [2, 4-5]. The supplementary parameter $\gamma=0.1$. The bootstrap filtering parameter is $r=8$, $\varepsilon=0.12$. The gain coefficient is $\beta=1$.

3.1 Analyzing transmission maps

3.1.1 Subjective analysis

The obtained transmission maps are compared with those obtained by other algorithms on the SOTS dataset and the ITS dataset, and the experimental results are shown in Figs.3 and 4.



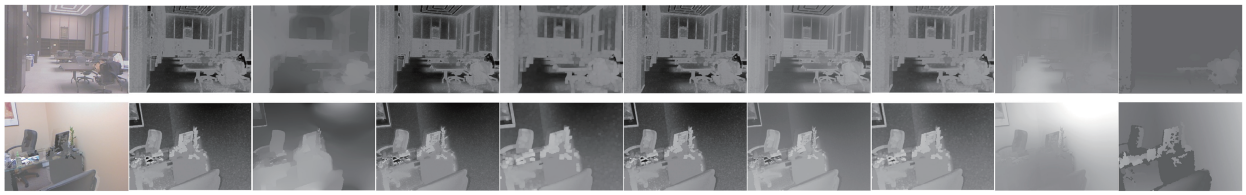
(a) Haze image (b) DCP[16] (c) Berman[21] (d) Ehsan[17] (e) Zhong[19] (f) Dwivedi[20] (g) Jin[23] (h) Balla[12] (i) Ours

Fig. 3 Transmission maps of different algorithms on SOTS dataset

It can be seen from Fig.3 that on the SOTS dataset, the transmission map generated by the DCP algorithm has high contrast but sometimes leads to over-enhancement, color distortion, and pseudo-edges. The transmission map of the Berman algorithm is too smooth, which leads to the loss of image details and edges. The transmission map of the Ehsan algorithm has average performance in terms of contrast and detail retention, and the image details are slightly blurred. The transmission maps of the Zhong algorithm and Jin algorithm are bright overall, resulting in overexposure of

the recovered image. The transmission map of the Dwivedi algorithm performs well in terms of detail retention and haze removal, but the contrast is low, and the haze effect is still present in some areas. The transmission map of the Balla algorithm shows signs of oversharpening, and despite the clarity of the image details, the overall appearance is unnatural, and there are some areas with haze effects. The transmission map of the Balla algorithm shows signs of oversharpening, overall appears unnatural, with artifacts and overexposure in some areas. The transmission map of the proposed algorithm on the SOTS dataset avoids the problem of too high or too low intensity values in the sky region, has a more uniform brightness and contrast, retains details well, and has no obvious overexposure or artifacts.

From Fig.4, it can be seen that the performance of the DCP algorithm, Berman algorithm, Ehsan algorithm, Jin algorithm, Dwivedi algorithm, and Balla algorithm on the ITS dataset is similar to that on the SOTS dataset. The Zhong algorithm performs better on the ITS dataset with sufficient detail retention, but there is a certain amount of overexposure. The transmission map of the proposed algorithm performs well on the ITS dataset with balanced brightness and contrast, good detail retention, and no obvious artifacts or overexposure problems.



(a) Haze image (b) DCP[16] (c) Berman[21] (d) Ehsan[17] (e) Zhong[19] (f) Dwivedi[20] (g) Jin[23] (h) Balla[12] (i) Ours (j) Given

Fig. 4 Transmission maps of different algorithms on ITS dataset

3.1.2 Objective analysis

However, visual quality is measured by the human visual system (HVS) and varies from person to person. Since the ITS dataset contains synthesized grayscale images and their transmission maps, this paper uses the root mean square error (RMSE) [30] for quantitative assessment of the ITS dataset. Table 1 shows 10 randomly selected images from the ITS dataset, comparing the RMSE values between a given transmission map and the transmission maps generated by different algorithms (The ideal value of RMSE is 0). Table 1 shows that the algorithm in this paper has lower RMSE values than the other algorithms in most cases. However, for image 2 and image 9, Jin algorithm outperforms the proposed algorithm. The overall results show that the RMSE value of the proposed algorithm is smaller, indicating that it is more effective than the other algorithms.

Table 1 RMSE values estimated by various algorithms for 10 images in ITS dataset

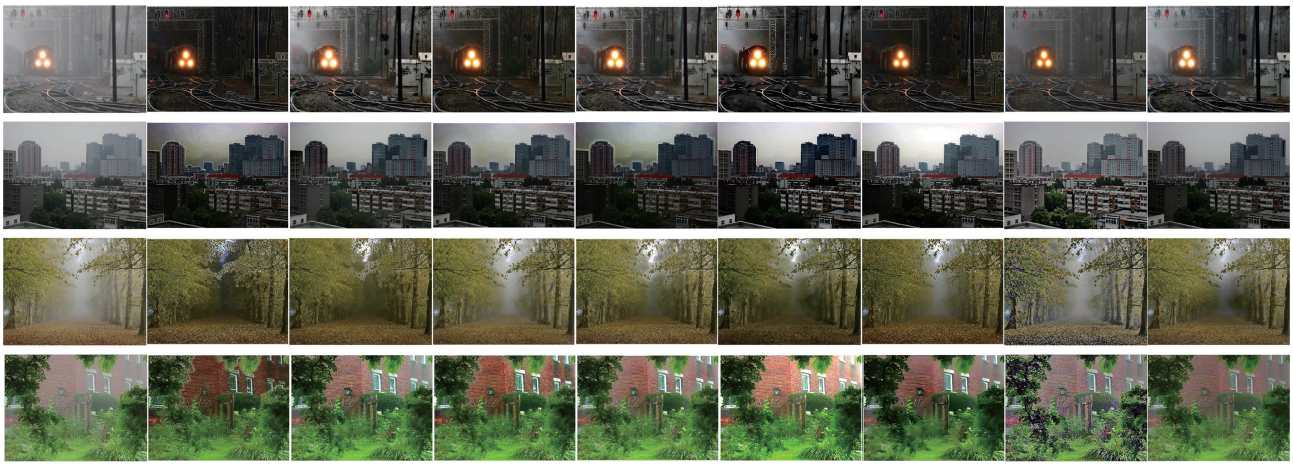
Image	RMSE							
	DCP[16]	Berman[21]	Ehsan[17]	Zhong[19]	Dwivedi[20]	Jin[23]	Balla[12]	Ours
Img1	0.055 0	0.052 6	0.062 7	0.042 7	0.032 7	0.072 6	0.046 2	**0.021 3**
Img2	0.041 6	0.059 2	0.053 8	0.039 7	0.026 1	**0.017 3**	0.023 9	0.024 3
Img3	0.047 8	0.027 2	0.067 7	0.025 7	0.018 2	0.062 8	0.025 2	**0.012 3**
Img4	0.048 2	0.078 5	0.052 6	0.038 2	0.032 7	0.032 7	0.024 6	**0.022 9**
Img5	0.040 1	0.033 7	0.078 2	0.065 3	0.047 9	0.052 6	0.042 5	**0.024 2**
Img6	0.039 8	0.027 4	0.027 4	0.028 3	0.062 7	0.065 2	0.053 2	**0.025 7**
Img7	0.019 7	0.056 3	0.053 6	0.066 3	0.018 1	0.072 8	0.016 2	**0.012 3**
Img8	0.025 5	0.052 8	0.027 3	0.066 7	0.022 3	0.052 6	0.016 2	**0.011 5**
Img9	0.027 8	0.024 2	0.062 7	0.022 7	0.022 6	**0.017 3**	0.028 3	0.021 6
Img10	0.033 9	0.033 6	0.046 3	0.047 6	0.022 4	0.024 1	0.027 4	**0.018 7**

3.2 Analyzing defogging results

3.2.1 Subjective analysis

Fig.5 shows the defogging results of different defogging algorithms on four typical foggy images. The DCP algorithm, the Ehsan algorithm, and the Jin algorithm eliminate most of the haze in the images but make the recovered images darker overall, with over-saturated colors and white edge defects and artifacts. As can be seen in Fig. 5(c), Berman algorithm does not process well in regions with high haze concentrations, and color distortion occurs. As shown in Fig. 5(e), the Chung algorithm recovers images with high brightness. As can be seen in Fig. 5(h), Balla algorithm results in oversharpening of the recovered image, such as parts of the building, leaves, and windows. As shown in Fig. 5(i), the proposed algorithm performs well in processing images containing large sky regions,

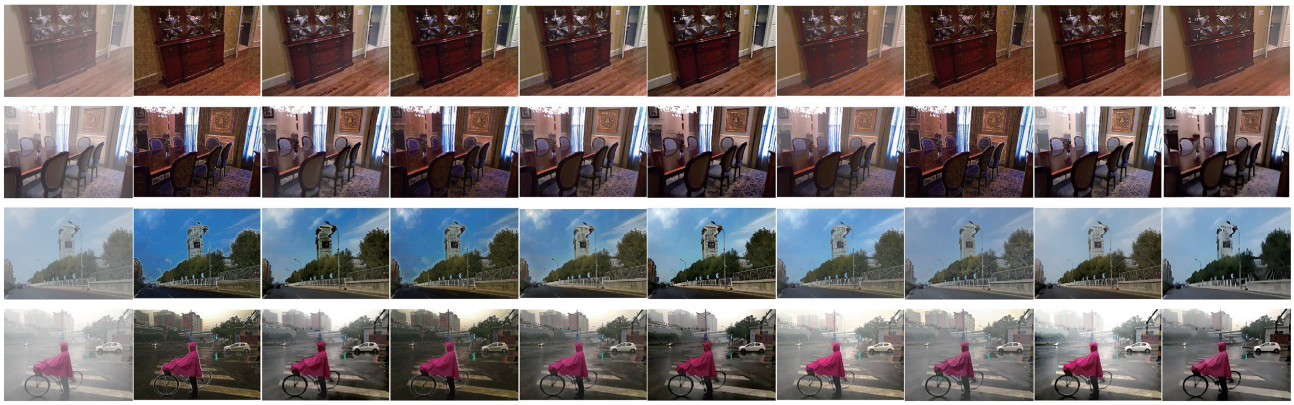
significantly improving the distortion problem in bright regions, while there is no halo effect in the sudden change of depth of field, which makes the recovered image closer to the real image.



(a) Haze image (b) DCP[16] (c) Berman[21] (d) Ehsan[17] (e) Zhong[19] (f) Dwivedi[20] (g) Jin[23] (h) Balla[12] (i) Ours

Fig. 5 Subjective evaluation on four typical foggy images

Fig. 6 demonstrates the results of the subjective evaluation of the proposed algorithm compared with other defogging algorithms on the SOTS dataset. Images from indoor and outdoor environments in this dataset are selected for the experiment, respectively. From Fig. 6(b) and 6(h), it can be observed that the DCP algorithm and Balla algorithm have an obvious over-enhancement problem in recovering the images, which leads to darker colors in the haze-free images and affects the detail quality. In the recovered images, the floor, tables, and chairs are darker than the real images. The color of the sky region is distorted, and the bicycle shows pseudo edges. The Berman algorithm fails to completely remove the haze residue on the crosswalk, which results in unclear details in the recovered image. As can be seen from Fig. 6(e) and 6(g), although the recovered images of Zhong algorithm and Jin algorithm perform well in terms of visual effect, their transmission map intensities are overall high, resulting in overexposure and loss of details. In contrast, the haze-free images restored by the proposed algorithm have no color distortion in the sky area. In the non-sky areas, there are clear details, the colors are moderate, and the restored images are closer to the real ones. Due to the powerful defogging capability of the DCP algorithm and the improvement of color distortion by the Berman algorithm, the restored images are closer to the original image, solving the problems of dull colors, overexposure, and appearance of artifacts in the restored image.



(a) Haze image (b) DCP[16] (c) Berman[21] (d) Ehsan[17] (e) Zhong[19] (f) Dwivedi[20] (g) Jin[23] (h) Balla[12] (i) Ours (j) Realimages

Fig. 6 Subjective evaluation on SOTS

Fig. 7 demonstrates the results of the subjective evaluation of the proposed algorithm compared with other defogging algorithms on the HSTS dataset. The DCP algorithm removes the haze to some extent. However, the image details are not clear enough, and the sky region shows large distortion and over-enhancement. Berman algorithm, Ehsan algorithm, and Zhong algorithm all generate visually appealing haze-free images, but the recovered image has a slight color bias from the real image, and the sky region also has a certain degree of distortion. Jin

algorithm, on the other hand, suffers from too much contrast and an overall over-enhancement, leading to the color distortion problem. As shown in Fig. 7(i), the proposed method has the best fog removal effect. There is no darkness or overexposure phenomenon. And the color of the forbidden city, trees, lake, and other dark objects is the most natural. There is no color distortion in the sky area, and the recovered image is closer to the real scene.



(a) Haze image (b) DCP[16] (c) Berman[21] (d) Ehsan[17] (e) Zhong[19] (f) Dwivedi[20] (g) Jin[23] (h) Balla[12] (i) Ours (j) Realimages

Fig. 7 Subjective evaluation on HSTS

3.2.2 Objective analysis

In this paper, we use various metrics such as average gradient (AG), information entropy (IE), edge intensity (EI), structural similarity index (SSIM), peak signal to noise ratio (PSNR), and patch-based contrast quality index (PCQI) for quantitative evaluation[31].

Table 2 demonstrates the average evaluation metrics of the defogging results of four natural foggy images. It shows that the proposed algorithm outperforms other algorithms in all five metrics. The EI value of the proposed algorithm is lower than Balla algorithm because Balla algorithm oversharpens the recovered image. The proposed algorithm performs well in terms of image defogging performance, generates recovered images that are sharper, contains richer information, and avoids severe distortion.

Table 2 Mean values of six unreferenced quantitative assessment metrics on naturally fogged image shown in Fig. 5

Algorithm	AG	IE	EI	SSIM	PSNR	PCQI
DCP[16]	5.328	5.273	45.276	0.736	15.628	0.762
Berman[21]	6.823	6.126	48.374	0.785	15.724	0.813
Ehsan[17]	5.433	5.162	47.872	0.737	15.726	0.874
Zhong[19]	6.873	6.384	47.823	0.726	15.677	0.863
Dwivedi[20]	7.726	6.863	48.827	0.826	16.163	0.927
Jin[23]	6.826	6.637	49.273	0.845	18.361	0.874
Balla[12]	6.972	6.829	**57.928**	0.826	18.233	0.973
Ours	**7.862**	**6.936**	53.876	**0.878**	**18.835**	**1.427**

Table 3 demonstrates the average evaluation metrics of the defogging results of the proposed algorithm and other defogging algorithms on the SOTS dataset.

Table 3 Mean values of six quantitative assessment metrics on SOTS dataset

Algorithm	AG		IE		EI		SSIM		PSNR		PCQI	
	Indoor	Outdoor	Indoor	Outdoor	Indoor	Outdoor	Indoor	Outdoor	Indoor	Outdoor	Indoor	Outdoor
DCP[16]	6.127	5.927	5.524	4.273	52.372	45.682	0.783	0.736	14.782	17.837	0.715	0.846
Berman[21]	6.762	6.846	5.926	5.837	54.827	49.726	0.785	0.726	15.623	17.724	0.827	0.734
Ehsan[17]	5.873	5.632	6.124	5.821	49.718	52.287	0.826	0.752	16.163	18.163	0.738	0.726
Zhong[19]	6.635	6.523	6.584	6.173	54.623	48.225	0.873	0.826	16.223	19.642	0.525	0.653
Dwivedi[20]	6.263	6.282	6.273	5.539	45.716	46.728	0.739	0.836	16.532	20.437	0.736	0.752
Jin[23]	6.391	6.891	**7.137**	**6.622**	65.284	56.628	0.863	0.872	16.762	21.361	1.013	0.854
Balla[12]	6.283	6.653	6.776	5.976	47.623	49.178	0.818	0.879	16.137	20.837	0.847	0.948
Ours	**7.854**	**7.954**	6.836	6.487	**73.539**	**68.862**	**0.898**	**0.937**	**18.835**	**22.627**	**1.154**	**1.263**

We select 50 indoor test images and 50 outdoor test images, respectively, and we can see that the proposed method achieves excellent results in most of the metrics, especially in AG, EI, PSNR, and PCQI. This indicates that the proposed method performs better in preserving the structural details of the original image and minimizes color distortion compared to the original image. Although it is slightly weaker than Jin algorithm in terms of IE, the images recovered by Jin algorithm suffer from gray-white bias and overexposure problems in general. Through the above objective comparisons and subjective evaluations, it is evident that the proposed method performs superiorly compared to other defogging methods, providing better quantitative assessment results while maintaining high subjective image quality.

Table 4 shows the average evaluation metrics of the

defogging results of the fogged image in Fig. 7. Compared with the other seven algorithms, the proposed algorithm achieves better results in all the indicators. The haze-free image recovered by the proposed algorithm has higher edge intensity values. The recovered haze-free image contains richer information and avoids serious distortion. Both objective and subjective comparisons show that the proposed method outperforms the other methods in terms of defogging effect and is able to recover clearer images.

Table 4 Mean values of six quantitative assessment metrics on HSTS dataset

Algorithm	AG	IE	EI	SSIM	PSNR	PCQI
DCP[16]	4.328	5.624	42.276	0.836	14.628	0.763
Berman[21]	5.823	5.226	56.374	0.728	15.744	0.896
Ehsan[17]	5.433	5.942	47.772	0.834	14.787	0.917
Zhong[19]	5.873	5.681	57.523	0.826	15.343	0.852
Dwivedi[20]	7.126	6.243	59.749	0.726	17.152	0.854
Jin[23]	6.326	5.621	59.256	0.872	16.411	0.852
Balla[12]	6.872	5.829	60.953	0.926	20.653	1.121
Ours	**7.562**	**6.936**	**67.876**	**0.948**	**21.835**	**1.217**

4 Conclusions

This paper proposes an image defoggin method that combines superpixel segmentation and transmission optimization to address common issues such as dark tones, artifact generation, and loss of image details during the dehazing process. The study shows that the proposed algorithm significantly improves the accuracy of atmospheric light values and the estimation accuracy of transmission rates. Regardless of the weather conditions, this algorithm performs well in dehazing and the experiments demonstrate its strong robustness. The algorithm in this paper performs better in preserving the structural details of the original image and eliminating artifacts. It solves the problems of overexposure and color distortion. The restored image is closer to the real image. To meet the real-time requirements of specific scenarios, this algorithm can be transplanted to an FPGA hardware development board to reduce running time. Moreover, this work can also be extended to real-time video dehazing to meet practical engineering needs.

Acknowledgement

I would like to express my gratitude to the reviewers and editors.

Declaration of conflicting interests

The authors have no conflict of interests related to this publication.

References

[1] GOYAL B, DOGRA A, LEPCHA D C, et al. Recent advances in image dehazing: Formal analysis to automated approaches. Information Fusion, 2024, 104: 102151.

[2] WANG C, ZHANG Q, ZHANG H. A novel image visibility detection algorithm based on improved nonlocal fog line prior. Journal of Sensing Technology, 2022, 35(3): 342-348.

[3] NING B, YANG M. Real time video defogging algorithm based on multi-scale guided filtering. Journal of North University of China (Natural Science Edition), 2024, 45(4): 439-447.

[4] JIN T H, TAO Y Y, LI Z Y. Improved algorithm for dark channel a priori defogging based on super-pixel image segmentation. Electronics Letters, 2023, 51(1): 146-159.

[5] FU, Q Q, JING, C L, PEI, Y L, et al. Research on detail enhancement algorithm for underwater images based on unsharpened mask-guided filtering. Journal of Oceanography, 2020, 42(7): 130-138.

[6] MOHAN S, SIMON P. Underwater image enhancement based on histogram manipulation and multiscale fusion. Procedia Computer Science, 2020, 171: 941-950.

[7] DUTTA M K, SARKAR R K. Application of Retinex and histogram equalisation techniques for the restoration of faded and distorted artworks: a comparative analysis. Optik, 2023, 272: 170201.

[8] GAMINI S, KUMAR S S. Homomorphic filtering for the image enhancement based on fractional-order derivative and genetic algorithm. Computers and Electrical Engineering, 2023, 106: 108566.

[9] BABU G H, ODUGU V K, VENKATRAM N, et al. Development and performance evaluation of enhanced image dehazing method using deep learning networks. Journal of Visual Communication and Image Representation, 2023, 97: 103976.

[10] MUNIRAJ M, DHANDAPANI V. Underwater image enhancement by combining color constancy and dehazing based on depth estimation. Neurocomputing, 2021, 460: 211-230.

[11] ZHANG J L, YANG Y. End-to-end defogging algorithm based on fog layer feature extraction and augmentation network. Journal of Measurement Science and Instrumentation, 2023, 14(1): 45-54.

[12] BALLA P K, KUMAR A, PANDEY R. A 4-channelled hazy image input generation and deep learning-based single image dehazing. Journal of Visual Communication and Image Representation, 2024, 100: 104099.

[13] WANG X G, TIAN J W, YU Y L, et al. A modified atmospheric scattering model and degradation image clarification algorithm for haze environments. Optics Communications, 2024, 560: 130489.

[14] FAN H W, ZHANG C, CAO X G, et al. A method for dust fog removal and enhancement of low illumination environmental images based on segmentation fusion of dark

and bright channels. Journal of Coal, 2024, 49(4): 2167-2178.
[15] XIE Y, JIA H Z, WANG T H, et al. A review of image defogging algorithms. Computer and Digital Engineering, 2022, 50(12): 2765-2774.
[16] HE K M, SUN J, TANG X O. Single image haze removal using dark channel prior//2009 IEEE Conference on Computer Vision and Pattern Recognition, June 20-25, 2009, Miami, FL, USA. New York: IEEE, 2009: 1956-1963.
[17] EHSAN S M, IMRAN M, ULLAH A, et al. A single image dehazing technique using the dual transmission maps strategy and gradient-domain guided image filtering. IEEE Access, 2021, 9: 89055-89063.
[18] HUA Z, DING Y J, LI J J. Image dehazing using near-infrared information based on dark channel prior. Procedia Computer Science, 2021, 187: 18-23.
[19] ZHONG H J, LIAO Y P. Image defogging algorithm based on improved dark channel and adaptive tolerance. Chinese Journal of Liquid Crystals and Displays, 2022, 37(11): 1488-1497.
[20] DWIVEDI P, CHAKRABORTY S. Single image dehazing using extended local dark channel prior. Image and Vision Computing, 2023, 136: 104747.
[21] BERMAN D, TREIBITZ T, AVIDAN S. Non-local image dehazing//2016 IEEE Conference on Computer Vision and Pattern Recognition, June 27-30, 2016, Las Vegas, NV, USA. New York: IEEE, 2016: 1674-1682.
[22] NIE X L, ZHANG C S, QIAN J B. Haze-lines optimized image defogging algorithm based on non-local prior. Journal of Optoelectronic. Laser, 2023, 34(2): 140-146.
[23] JIN K, LI G, ZHOU L, et al. Image dehazing using non-local haze-lines and multi-exposure fusion. Journal of Visual Communication and Image Representation, 2024, 101: 104145.
[24] HUANG W, WEI Y. Single image dehazing via color balancing and quad-decomposition atmospheric light estimation. Optik, 2023, 275: 170573.
[25] YADAV S K, SARAWADEKAR K. Robust multi-scale weighting-based edge-smoothing filter for single image dehazing. Pattern Recognition, 2024, 149: 110137.
[26] DI S H, LIAO M, ZHAO Y Q, et al. Image superpixel segmentation based on hierarchical multi-level LI-SLIC. Optics & Laser Technology, 2021, 135: 106703.
[27] LIANG H L, WANG Z Q, CUI P. Adaptive SLIC super-pixel segmentation algorithm based on Pearson's correlation coefficient. Software Engineering, 2024, 27(3): 30-35.
[28] KARIM S, TONG G, LI J Y, et al. Current advances and future perspectives of image fusion: a comprehensive review. Information Fusion, 2023, 90: 185-217.
[29] LI B Y, REN W Q, FU D P, et al. Benchmarking single-image dehazing and beyond. IEEE Transactions on Image Processing, 2019, 28(1): 492-505.
[30] SAHU G, SEAL A, KREJCAR O, et al. Single image dehazing using a new color channel. Journal of Visual Communication and Image Representation, 2021, 74: 103008.
[31] KUMARI A, SAHOO S K. A new fast and efficient dehazing and defogging algorithm for single remote sensing images. Signal Processing, 2024, 215: 109289.

结合SLIC超像素分割和透射率优化的图像去雾算法

李积英*, 刘　钰, 刘　洁

兰州交通大学 电子与信息工程学院, 甘肃 兰州 730070

摘　要： 在雾霾条件下拍摄图像时，光线因受到粒子散射而发生衰减和偏转，导致亮度降低和色彩失真，影响了视觉系统的成像质量。本文提出了一种结合超像素分割和透射率优化的去雾方法。首先，利用颜色熵计算雾霾图像的复杂度，自适应确定超像素块的数量。采用简单线性迭代聚类(SLIC)超像素分割方法获得具有相同特征的超像素块，选择得分最高的超像素块作为候选块，精确估计大气光值。然后，利用多尺度暗通道先验和非局部雾线先验估计透射率，再通过小波变换得到融合后的初始透射率。此外，本文引入了基于非锐化掩模的引导滤波，进一步提高了透射估计精度。最后，采用大气散射模型对无雾图像进行反演。本文在三个数据集上进行了大量的定量和定性实验。实验结果表明，本文算法可以取得较好的去雾效果，尤其在天空区域图像复原效果方面较为突出。

关键词： 超像素块；大气光值；多尺度暗通道先验；非局部雾线先验；透射率融合；非锐化掩模

引用格式： LI Jiying, LIU Yu, LIU Jie. Image defogging algorithm combining SLIC super-pixel segmentation and transmission optimization. Journal of Measurement Science and Instrumentation, 2026, 17(2): 267-277. DOI: 10.62756/jmsi.1674-8042.2026023